

Anisotropy of Pb L_3 -subshell x rays excited by low-velocity-proton impact

C. V. Barros Leite, N. V. de Castro Faria, R. J. Horowicz, E. C. Montenegro,
and A. G. de Pinho

Department of Physics, Pontifícia Universidade Católica do Rio de Janeiro, RJ 22453, Brasil

(Received 3 September 1981)

The anisotropy of the resolved Ll x-ray line emitted from proton-excited Pb atoms has been measured. The anisotropy coefficient is strongly dependent on the projectile energy within the proton energy range studied (from 0.4 to 3.0 MeV). A detailed explanation of this energy dependence is suggested in terms of the Coulomb interaction of the projectile with the target nucleus. The deflection effect is discussed in earlier publications; the retardation effect is introduced here for the first time in the context of the alignment of L_3 -subshell vacancies. Both effects are treated with appropriate weight functions for the different magnetic substates of the L_3 subshell.

I. INTRODUCTION

When an atom is ionized in one of its inner shells, the electrons rearrange themselves to fill the vacancy, with the transition energy released as a photon or transferred to an outer electron. A collimated beam of unpolarized charged particles impinging upon unpolarized target atoms is able to create vacancies which, if produced in subshells with total angular momentum $j > \frac{1}{2}$, can "remember" the direction of incidence of the beam. The following x-ray or Auger electron may have a non-isotropic angular distribution. In addition, the x rays should also be linearly polarized.¹⁻⁴ Effects of this process of alignment have been extensively investigated in the past decade.⁵⁻¹⁵

Dipole radiation resulting from the transition of an electron from the magnetic substates defined by quantum numbers j_f, m_f to the aligned vacancy substates j_i, m_i created by a collimated beam of heavy charged particles, which are not observed after scattering, exhibits the following pattern^{1,2,16}:

$$W_{j_i, j_f, E}^{(\theta)} = \frac{W_T}{4\pi} [1 + A(j_i, j_f, E) P_2(\cos\theta)], \quad (1)$$

where E is the beam energy, θ denotes the angle between emitted x ray and z axis, the last being the direction of incidence of the particle beam, and W_T is the total intensity emitted into the 4π solid angle.

For an initial vacancy created in the $L_3(2p_{3/2})$

subshell,

$$A\left(\frac{3}{2}, j_f, E\right) = \alpha(j_f) \mathcal{A}_2(E), \quad (2)$$

where $\alpha = \frac{1}{2}$, $\frac{1}{10}$ and $-\frac{2}{5}$ for Ll , $L\alpha_1$, and $L\alpha_2$ transitions, respectively, i.e., for electrons coming from the $3s_{1/2}$, $3d_{5/2}$, and $3d_{3/2}$ subshells, respectively, and

$$\mathcal{A}_2(E) = \frac{\sigma_{3/2}(E) - \sigma_{1/2}(E)}{\sigma_{3/2}(E) + \sigma_{1/2}(E)} = \frac{\sigma_1(E) - \sigma_0(E)}{2\sigma_1(E) + \sigma_0(E)}, \quad (3)$$

where $\sigma_{1/2, 3/2}$ and $\sigma_{0,1}$ are cross sections of magnetic subshells of an L_3 and a $2p$ electron, respectively. Calculations of σ_m are model dependent. Explicit integral, analytical expressions in the frame of the PWBA with screened hydrogenic wave functions are given by McFarlane¹⁷ and by Kamiya *et al.*¹³

If the radiation following the creation of a $2p_{3/2}$ vacancy is observed, one cannot distinguish if the vacancy was directly produced by ionization or if it was transferred to $2p_{3/2}$ after the ionization of an inner subshell. All these subshells have $j = \frac{1}{2}$; therefore the transferred vacancies are not aligned and the observed anisotropy of the x rays is attenuated. Neglecting the contribution of K -shell vacancies one defines¹⁰

$$\mathcal{A}'_2 = F \mathcal{A}_2, \quad (4)$$

with the energy-dependent attenuation factor given by

$$F = \left[1 + f_{23} \frac{\sigma^2}{\sigma^3} + (f_{13} + f_{12}f_{23}) \frac{\sigma^1}{\sigma^3} \right]^{-1}, \quad (5)$$

where the f_{ij} are the L -shell Coster-Kronig transition rates, and the σ^i are the total ionization cross sections in the three L_i subshells. It is well known that for the ionization of heavy atoms by protons, there is a dramatic rise in the σ^1/σ^3 ratio whenever the incident energy falls below 1 MeV. Therefore a severe attenuation in the anisotropy is to be expected at very low impact energies.

As the bombarding energy decreases, the \mathcal{A}_2 anisotropy coefficient [Eq. (3)] can be shown to converge asymptotically to a constant value. The effect of the attenuation factor is to produce a broad minimum in the \mathcal{A}'_2 versus E curve (see Sec. III).

The PWBA calculation of the ionization cross sections is best expressed in terms of the scaled energy η and scaled binding energy θ_i . In the adiabatic region the scaled cross section is a universal function¹⁸ of η/θ_i^2 . Obviously \mathcal{A}_2 [Eq. (3)] is also a universal function of η/θ_3^2 but \mathcal{A}'_2 is not since the f_{ij} 's are Z dependent.

Recently Pálincás *et al.*^{14,15} have measured the anisotropy coefficient in gold with collimated proton beams with energies ranging from 250 up to 1500 keV. They emphasized that the factor F is not enough to take into account the observed attenuation and suggested¹⁴ that the deflection of the projectile by the Coulomb field of the target nucleus is at the origin of this more pronounced attenuation.

A coefficient \mathcal{A}'_2 was defined in Ref. 14 as

$$\mathcal{A}'_2 = \langle P_2(\cos\omega) \rangle \mathcal{A}'_2, \quad (6)$$

where ω is the scattering angle of the projectile. The average value was calculated with the weight function given by Brandt and Lapicki,¹⁹ in the impact-parameter formulation, for the L_3 subshell. Those authors¹⁴ interpret this procedure as the choice of the axis of alignment, not in the direction of the incoming projectile, but in the direction of the outgoing particle.

Jitschin *et al.*²⁰ have also suggested considering the Coulomb deflection effect by using the tangent line to the hyperbolic trajectory at the distance of closest approach. The average value was calculated with the same weight function¹⁹ for both substates.

In this case the anisotropy coefficient will be given by

$$\mathcal{A}'_2 = \langle P_2[\cos(\omega/2)] \rangle \mathcal{A}'_2. \quad (7)$$

In this paper we report measurements of the anisotropy of the Ll line emitted by Pb atoms bombarded by protons with energies from 400 to 3000 keV. A discussion of the effect of the Coulomb field of the target nucleus on the angular distribution of the radiation is presented.

II. EXPERIMENT

Beams of H^+ were produced at the PUC/RJ 4-MV Van de Graaff accelerator. The beam was directed into a target at 45° with respect to its axis by a pair of tantalum collimators, 3 cm apart, both with a diameter of 1.5 mm. The current was kept below 150 nA to avoid pileup and the deterioration of the target. The x rays passed the chamber windows consisting of a 6- μm Mylar foil and were detected outside the vacuum chamber by a movable Si(Li) detector having an energy resolution of 180 eV (FWHM) at 5.9 keV. A collimating system in front of the x-ray detector was provided with thin Al foils to absorb the strong M x rays from the target. In our scattering chamber 4-mm diameter holes allowed the observation of the x rays at angles from 10° up to 90° at 10° intervals, and at 115° , 130° , and 145° . Targets with a thickness of approximately $100 \mu\text{g}/\text{cm}^2$ were made by vacuum evaporation of Pb onto thin formvar films. As a test the $K\beta/K\alpha$ intensity ratio of Cu x rays was measured and isotropy was found to within an error of 3%. This puts an upper limit for the anisotropy we were able to measure.

In order to reach statistical errors less than 3% in the area of the Ll peak each run lasted typically 6 hours at very low impact energies. A critical problem was the background subtraction, and a careful analysis of each spectrum was undertaken by graphical hand methods.

Since the lines of the $L\gamma$ x-ray group result from initial $j = \frac{1}{2}$ vacancies, this group is expected to be isotropic and thus it is usual^{10,14} to take its intensity to normalize the intensities of the anisotropically emitted lines. Therefore the $Ll/L\gamma$ intensity ratio has the same angular distribution as the Ll line. Since Eq. (1) gives the intensity ratio as a linear function of $\cos^2\theta$, the slope obtained by a least-squares fit provided an easy determination of the anisotropy coefficient. However, we preferred to use the $Ll/L\alpha$ intensity ratio to obtain the value of \mathcal{A}'_2 . In this case the problem of background subtraction is considerably reduced and statistical errors are significantly less.

From Eqs. (1), (2), and (4) it follows that

$$\frac{W_l}{W_\alpha}(\theta) = \frac{W_{T,l}}{W_{T,\alpha}} \times \frac{1 + \frac{1}{2} \mathcal{A}'_2 P_2(\cos\theta)}{1 + \left[\frac{1}{10} \frac{W_{T,\alpha_1}}{W_{T,\alpha}} - \frac{2}{5} \frac{W_{T,\alpha_2}}{W_{T,\alpha}} \right] \mathcal{A}'_2 P_2(\cos\theta)} \quad (8)$$

The experimental values of the anisotropy parameter \mathcal{A}'_2 as a function of the incident energy were obtained from Eq. (8). Partial radiative widths for the $L\alpha$ lines given by Scofield²¹ were used.

Figures 1 and 2 show representative x-ray energy spectrum and angular distribution of the $Ll/L\alpha$ ratio, respectively.

Our experimental values of \mathcal{A}'_2 are given in Table I. For the attenuation factor F , use was made of experimental values of the σ^2/σ^3 and σ^1/σ^3 cross-section ratios obtained in our laboratory and of values of the Coster-Kronig transition rates tabulated by Krause.²² In Fig. 3 the experimental curve F versus η/θ_3^2 is compared with those obtained with the same values of f_{ij} and with theoretical ionization cross sections, one in the strict PWBA framework, the other with binding, trajectory, and relativistic corrections.²³ The experimental values of \mathcal{A}'_2 are presented in Fig. 4 together with the published values of Jitschin *et al.*¹⁰ and of Pálinkás *et al.*^{14,15} They agree quite well with each other, but it is evident that they deviate from the \mathcal{A}'_2 values obtained from the PWBA results for \mathcal{A}'_2 and the experimental F factor. For Au ($Z=79$) and Pb ($Z=82$) the calculated \mathcal{A}'_2 curves are not distinguishable. The solid curve labeled $\mathcal{A}'_2^{\text{ATSL}}$ (where ATSL stands for averaged tangential straight line) is defined in Sec. III B where the influence of the Coulomb repulsion of the projec-

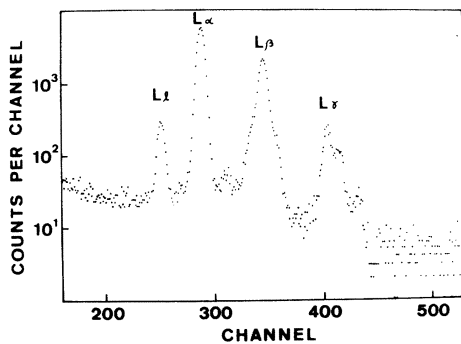


FIG. 1. X-ray energy spectrum for 650-keV proton impact on lead observed at $\theta=40^\circ$.

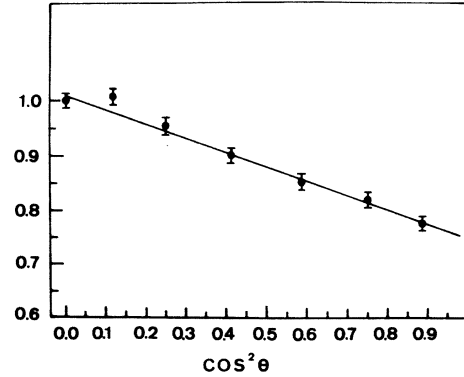


FIG. 2. Measured intensity ratio I_α/I_l as a function of $\cos^2\theta$. The bombarding energy was 650 keV and the data were normalized to unity at $\theta=0^\circ$. The straight line is a best fit to the function $\cos^2\theta$.

tile by the target nucleus on the observed anisotropy will be discussed.

III. DISCUSSION AND CONCLUSIONS

A. Predictions of the PWBA

Starting from the results given by McFarlane¹⁷ and by Kamiya *et al.*¹³ in the frame of the PWBA and with screened hydrogenic wave functions, it is easy to show that the low-velocity behavior of σ_0 is given by

$$\sigma_0 \simeq (2^{38} \times 9/77) \pi a_0^2 (Z_1/Z_2)^2 \eta^5 \theta_3^{-11}, \quad (9)$$

and that σ_1 converges to $\sigma_0/12$. In the above expression $Z_1 e$ is the projectile charge, $Z_2 e$ is the ef-

TABLE I. Measured values of the anisotropy parameter \mathcal{A}'_2 and the resulting value of \mathcal{A}'_2 given by \mathcal{A}'_2/F .

E (keV)	\mathcal{A}'_2 (%)	\mathcal{A}_2 (%)
400	-31(10)	-46(12)
460	-35(9)	-49(11)
500	-31(6)	-42(8)
570	-33(5)	-43(6)
650	-32(3)	-40(4)
800	-35(3)	-41(4)
1000	-34(3)	-38(4)
1250	-29(3)	-32(4)
1500	-20(3)	-22(4)
2000	-10(2)	-11(3)
2500	-5(3)	-6(4)
3000	+6.5(4.0)	+8(5)

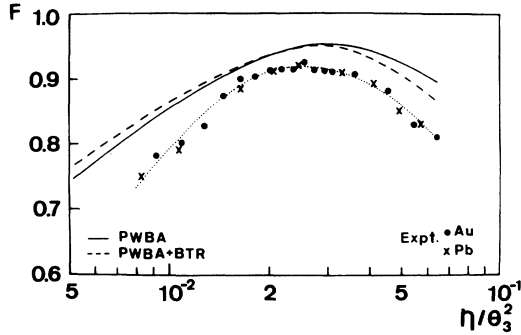


FIG. 3. Experimental values of F as a function of η/θ_3^2 . Solid curve: PWBA calculations; broken curve: PWBA with binding, trajectory, and relativistic corrections (Ref. 23). The theoretical curves for Au and Pb are not distinguishable. The dotted curve among the experimental points is merely a guide to the eyes. The experimental errors are not represented. They are estimated to be $\sim 5\%$ for η/θ^2 up to $\sim 1 \times 10^{-2}$, and then $\sim 3\%$.

fective charge as seen by an electron of the L subshell of the target atom, and a_0 is the fundamental Bohr radius.

Therefore the prediction of the PWBA at the extreme adiabatic limit is a constant value of \mathcal{A}_2 .

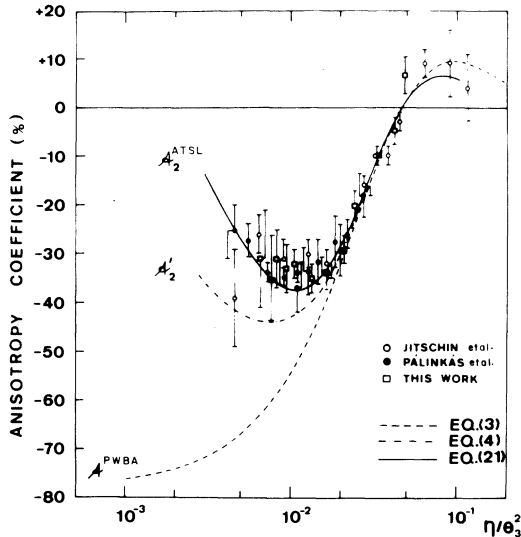


FIG. 4. Measured values of the anisotropy parameter compared with theoretical predictions: Curve \mathcal{A}_2 is a representation of Eq. (3) calculated in the PWBA, curve \mathcal{A}'_2 is the preceding curve corrected for Coster-Kronig transitions with the factor F obtained from interpolated or extrapolated experimental points for the σ^i cross sections, and the tabulated Krause's values for the f_{ij} coefficients. The solid curve $\mathcal{A}_2^{\text{ATSL}}$ is a representation of Eq. (21).

From Eq. (3), it follows that $\mathcal{A}_2 \rightarrow -11/14$. On the other hand, at the same limit, the attenuation factor converges asymptotically to the expression

$$F = \left[1 + \frac{1}{2} \left(\frac{\theta_3}{\theta_2} \right)^{11} f_{23} + \frac{11}{720} \left(\frac{\theta_3}{\theta_1} \right)^{11} (f_{13} + f_{12} f_{23}) \frac{\theta_1^2}{\eta} \right]^{-1}. \quad (10)$$

Of course when the incident energy is barely sufficient to ionize the L_3 subshell but it is yet smaller than the binding energies of the inner subshells, the factor F rises abruptly to one since in this case there will be no unaligned vacancies transferred to L_3 .

As a result, it can be predicted in the strict PWBA framework that the \mathcal{A}'_2 versus η/θ_3^2 curve must present a broad minimum at about $\eta/\theta_3^2 \approx 7 \times 10^{-3}$ for the heaviest atoms ($Z \geq 79$). This minimum corresponds to a negative anisotropy $\mathcal{A}'_2 \approx 50\%$. Binding, trajectory, and relativistic corrections do not alter in a significant way this general prediction of the PWBA. Experimentally we observe that the minimum is displaced to higher values of η/θ_3^2 , that the curvature is more pronounced, and that the maximum absolute value of \mathcal{A}'_2 is smaller.

Obviously care must be taken in extrapolating PWBA predictions to extreme low values of η . The numerical calculations of the cross sections are performed with approximate limits of integration that do not take into account in an exact way the conservation laws.¹⁸ In particular, all the cross sections must go to zero at the threshold, the upper and lower limits of the integrations over the transferred momentum and energy becoming equal to each other in both cases.

Independent of the correctness of the limits of integration, one cannot expect that the PWBA will give valuable results near the threshold. On the other hand, the anisotropy and/or polarization of the emitted photon in this extreme limit is a controversial matter and will depend on details of the process^{24,2} (e.g., if the projectile excites or ionizes the target and, in this second case, if the inner-shell electron is ejected or captured by the bare projectile).

B. Deflection and retardation effects

If the reduced de Broglie wavelength of the proton is small compared with the Bohr radius of the

electron to be ejected, a classical hyperbolic trajectory will describe the movement of the projectile in the field of the target nucleus. The ionization can occur at any point of the trajectory and the relevant direction is that of the average proton velocity along the classical trajectory. If the intensity of the emitted radiation is measured with respect to the incoming beam direction, the resulting pattern will depend upon the angle between the average direction of \vec{v} and the incoming direction. The average direction is that of the tangent at the point of closest approach to the atomic nucleus.²⁰ The straight-line path approximation is maintained but, since for each bombarding energy there is an infinite family of trajectories each one characterized by an impact parameter, to maintain the straight-line path approximation an average over these impact parameters is to be taken.

However, better agreement is obtained between the experimental data and the \mathcal{A}'_2 curve than with the \mathcal{A}''_2 curve (see Fig. 5). This is a fortuitous result and it would be essential to consider different weight functions for each magnetic substate in order to improve the situation.

In fact, the hypothesis of equal weight functions for different substates is not physically justifiable.

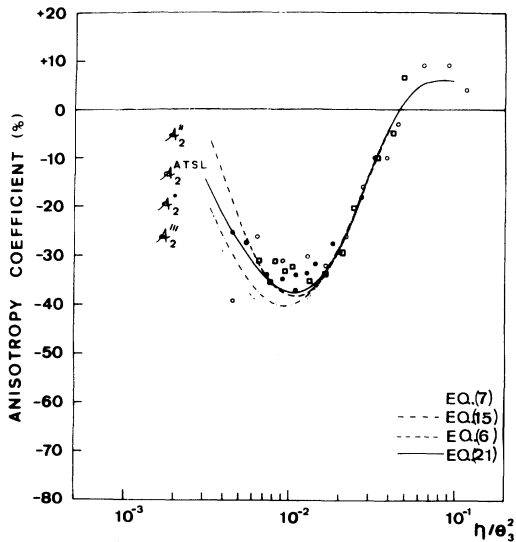


FIG. 5. Comparison among suggested explanations for the attenuation of the anisotropy at low impact velocities. The same experimental points of Fig. 4 are reproduced without the error bars. \mathcal{A}'_2 represents Eq. (6) proposed in Ref. 14, \mathcal{A}''_2 represents Eq. (7), \mathcal{A}^*_2 represents Eq. (15), and \mathcal{A}^{ATSL}_2 represents Eq. (21). They were calculated with the same factor F and for $Z_2=82$. Curves for $Z_2=79$ differ no more than 4% from the curves showed.

For the $m=0$ and $m = \pm 1$ substates of the $2p$ subshell, the normalized weight functions are given in the adiabatic limit by²⁵

$$W_0(x) = (7/1152)x^6 [K_3(x)]^2 \tag{11}$$

and

$$W_1(x) = (7/192)x^6 [K_2(x)]^2, \tag{12}$$

where K_n denotes the modified Bessel function of order n .

Analytical approximations of the weight functions were obtained following the same procedure adopted by Brandt and Lapicki¹⁹ giving

$$W_0(x) = (7/18)(1 + 2x + 2x^2 + 0.8x^3 + 0.16x^4 + \frac{1}{128}\pi x^5)e^{-2x} \tag{13}$$

and

$$W_1(x) = (7/48)(1 + 1.96x + 1.52x^2 + \frac{1}{8}\pi x^3)x^2 e^{-2x}, \tag{14}$$

respectively. The argument x is equal to pq_0 , where p is the classical parameter of impact and $\hbar q_0$ is the minimum momentum transfer. These approximations are shown in Fig. 6. With the half distance of closest approach given by $d = Z_1 Z_2 e^2 / 2E$ we have $\omega/2 = \cot^{-1}(p/d)$. Then a better approximation for the anisotropy coefficient will be given by

$$\mathcal{A}^*_2 = \frac{4F}{3\sigma^3} [\sigma_1 \langle P_2(\cos(\omega/2)) \rangle_1 - \sigma_0 \langle P_2(\cos(\omega/2)) \rangle_0], \tag{15}$$

where $\langle \rangle_1$ and $\langle \rangle_0$ represent averages calculated with the functions W_1 and W_0 , respectively. As in Refs. 14 and 20, an approximation is implicit in the averaging process.

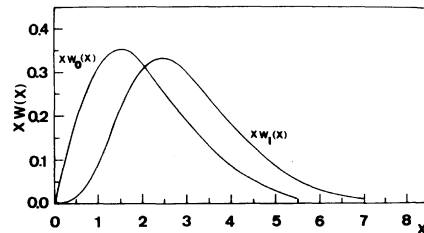


FIG. 6. Functions $xW_m(x)$ for $m=0$ and $m=1$. Mean values of x are $\langle x \rangle_0 = 2.16$ and $\langle x \rangle_1 = 3.00$, respectively.

After integrating over the azimuthal angle, the integral over the impact parameter is performed with the assumption that

$$d\sigma_m = \sigma_m x W_m(x) dx .$$

The integration over x is then reduced to the determination of the average value of $P_2(\cos[\omega(x)/2])$, namely,

$$\int_0^\infty P_2(\cos[\omega(x)/2]) x W_m(x) dx \\ = \int_0^\infty \frac{2x^2 - (dq_0)^2}{2[x^2 + (dq_0)^2]} x W_m(x) dx . \quad (16)$$

In Fig. 5, curve \mathcal{A}_2^* represents Eq. (15).

Besides the "rotation" of the radiation pattern produced by the deflection of the ionizing projectile in the Coulomb field of the target nucleus, it is evident that a retardation effect is present which is different in the $m=0$ and the $m=\pm 1$ substates.

In the hyperbolic trajectory the velocity v_{\min} at the distance of closest approach is given in terms of the incident velocity by

$$v_{\min} = v_1 [(\epsilon - 1)/(\epsilon + 1)]^{1/2} , \quad (17)$$

with

$$\epsilon = [(p/d)^2 + 1]^{1/2} .$$

$$\mathcal{A}_2^{\text{ATSL}} = F \frac{\sigma_1^* \langle P_2(\cos(\omega/2)) \rangle_1 - \sigma_0^* \langle P_2(\cos(\omega/2)) \rangle_0}{2\sigma_1^* + \sigma_0^*} , \quad (21)$$

where σ_m^* is the ionization cross section for the magnetic m substate calculated in the PWBA with the effective reduced energy η_m^* . The anisotropy coefficient calculated for $Z=82$ is shown in Figs. 4 and 5 by the solid line curves. Note that two kinds of averages have been performed. Firstly, we considered the average, both in direction and in magnitude of the vector \vec{v} along the trajectory. The average direction is that at the vertex of the hyperbola; the average magnitude was adopted as being the arithmetic mean between the incident and the minimum values. Secondly, an average over the impact parameters was computed for each incident energy with the appropriate weight function for each magnetic substate. We maintain, however, the basic PWBA formulation for calculating the partial ionization cross sections. Even if the use of an effective value of η does not give the best absolute Coulomb retardation correction,²⁶ it is important to note that the anisotropy does not

Following Kocbach,²⁶ the retardation effect introduced by the Coulomb field of the target nucleus is best described by adopting the arithmetic mean between v_1 and v_{\min} . Even if this choice of the average value of the speed along the classical trajectory does not reproduce quite well the absolute values of the cross sections, it must be noted that \mathcal{A}_2 is expressed in terms of the ratio σ_0/σ_1 . We expect that a good estimate of the differential effect introduced by the unequal weight functions W_m can be obtained introducing the concept of effective reduced energies η_m^* .

We define

$$\langle v_{\min} \rangle_m = v_1 \langle [(\epsilon - 1)/(\epsilon + 1)]^{1/2} \rangle_m \quad (18)$$

and

$$\langle \bar{v} \rangle_m = (v_1 + \langle v_{\min} \rangle_m) / 2 , \quad (19)$$

the two different average values being given by

$$\langle [(\epsilon - 1)/(\epsilon + 1)]^{1/2} \rangle_m \\ = \int_0^\infty \frac{x^2 W_m(x) dx}{dq_0 + [(dq_0)^2 + x^2]^{1/2}} . \quad (20)$$

Since η_m^* is proportional to $\langle \bar{v} \rangle_m^2$ we get finally

depend on the absolute values of σ_m but depends only on the ratio σ_0/σ_1 . We expect that the different effects of Coulomb retardation on the magnetic substates $m=0$ and $|m|=1$ is adequately taken into account in the cross-section ratio. The binding effect that is also described in the impact-parameter formulation¹⁹ is one order of magnitude less than the retardation effect in the energy interval we are especially interested in ($E_p \lesssim 1$ MeV). For this reason it was not considered. The agreement with the experimental results is satisfactory.

Coincidence experiments where a given impact parameter could be selected would shed more light on the mechanism of alignment of the vacancies eliminating the complications introduced by the need of averaging over the scattering angle. In an angular correlation experiment the inaccuracies introduced by poor statistics will be compensated by the possibility of observing much greater anisotropies.

ACKNOWLEDGMENTS

This research was supported in part by the Conselho Nacional de Pesquisa do Brasil and by the

Financiadora de Estudos e Projetos. The authors wish to thank Dr. E. F. da Silveira for helpful discussions.

-
- ¹E. G. Berezhko and N. M. Kabachnik, *J. Phys. B* **10**, 2467 (1977).
- ²V. V. Sizov and N. M. Kabachnik, *J. Phys. B* **13**, 1601 (1980).
- ³B. Cleff and W. Mehlhorn, *J. Phys. B* **7**, 593 (1974).
- ⁴B. Cleff and W. Mehlhorn, *J. Phys. B* **7**, 605 (1974).
- ⁵J. Hrdy, A. Henins, and J. A. Bearden, *Phys. Rev. A* **2**, 1708 (1970).
- ⁶E. Döbelin, W. Sandner, and W. Mehlhorn, *Phys. Lett.* **49A**, 7 (1974).
- ⁷M. Rodbro, R. DuBois, and V. Schmidt, *J. Phys. B* **11**, L551 (1978).
- ⁸A. Schöler and F. Bell, *Z. Phys. A* **286**, (1978).
- ⁹V. P. Petukhov, E. A. Romanovsky, N. M. Kabachnik, V. V. Sizov, and S. V. Ermakov, in *Abstracts of the Eleventh ICPEAC, Kyoto, 1979*, edited by K. Takayanagi and N. Oda (The Society for Atomic Collision Research, Kyoto, 1979), p. 668.
- ¹⁰W. Jitschin, H. Kleinpoppen, R. Hippler, and H. O. Lutz, *J. Phys. B* **12**, 4077 (1979).
- ¹¹M. Aydinol, R. Hippler, I. McGregor, and H. Kleinpoppen, *J. Phys. B* **13**, 989 (1980).
- ¹²N. M. Kabachnik, V. P. Petukhov, E. A. Romanovskii, and V. V. Sizov, *Zh. Eksp. Teor. Fiz.* **78**, 1733 (1980) [*Sov. Phys.—JETP* **51**, 869 (1980)].
- ¹³M. Kamiya, Y. Kinefuchi, H. Endo, A. Kuwako, K. Ishii, and S. Morita, *Phys. Rev. A* **20**, 1820 (1979).
- ¹⁴J. Pálincás, L. Sarkadi, and B. Schlenk, *J. Phys. B* **13**, 3829 (1980).
- ¹⁵J. Pálincás, B. Schlenk, and A. Valek, *J. Phys. B* **14**, 1157 (1981).
- ¹⁶N. F. Mott and H. S. W. Massey, *Theory of Atomic Collisions* (Oxford University Press, New York, 1965) 3rd ed.
- ¹⁷S. C. McFarlane, *J. Phys. B* **5**, 1906 (1972).
- ¹⁸E. Merzbacher and H. W. Lewis, *Handbuch der Physik* (Springer, Berlin, 1958), Vol. 34, p. 166.
- ¹⁹W. Brandt and G. Lapicki, *Phys. Rev. A* **10**, 474 (1974).
- ²⁰W. Jitschin, H. O. Lutz, and H. Kleinpoppen, International Conference on X-ray Processes and Inner-Shell Ionization, Stirling, 1980, Abstract No. 32 (in press).
- ²¹J. H. Scofield, *At. Data Nucl. Data Tables* **14**, 121 (1974).
- ²²M. D. Krause, *J. Phys. Chem. Ref. Data* **8**, 307 (1979).
- ²³W. Brandt and G. Lapicki, *Phys. Rev. A* **20**, 465 (1979).
- ²⁴W. Sandner and W. Schmitt, *J. Phys. B* **11**, 1833 (1978).
- ²⁵E. C. Montenegro and A. G. de Pinho, *Rev. Bras. Fis.* (in press).
- ²⁶L. Kocbach, *Phys. Norv.* **8**, 187 (1976).